Effect of phase difference on the interaction of hairpin vortices induced by in-line twin synthetic jets

Xin Wen[1], Hui Tang[2, c]

[1]School of Mechanical and Aerospace Engineering, Nanyang Technological University, Singapore 639798, Singapore
[2]Department of Mechanical Engineering, The Hong Kong Polytechnic University, Kowloon, Hong Kong SAR, China
[c]Corresponding author: Tel.: +852-27667815; Fax: +852-23654703; Email: h.tang@polyu.edu.hk

Abstract An experimental study is carried out to investigate the effect of operational phase difference of in-line twin synthetic jet actuators (SJAs) on the interaction of synthetic-jet-induced hairpin vortices. The resulting vortex structures at four phase differences, i.e., $\Delta\phi = 0°$, $90°$, $180°$, and $270°$, are presented and compared using both stereo dye visualization and particle image velocimetry (PIV) measurements. Three types of vortex structures are observed: *one combined vortex* at $\Delta\phi = 90°$, *two completely separated hairpin vortices* at $\Delta\phi = 270°$, and *partially interacting vortex structures* at $\Delta\phi = 0°$ and $180°$. The combined vortex is the strongest and most penetrates into the boundary layer. The completely separated hairpin vortices are the closest to the wall and hence are able to exert the most influence in the near-wall region. As for the partially interacting vortex structures, the head of one hairpin vortex interacts with legs of the other, producing complex vortex structures. Through this study it is also found that hairpin vortices issued from the upstream SJA are able to maintain their coherence more easily than their counterparts issued from the downstream SJA, regardless the phase difference. The secondary vortices captured by the PIV measurements are also compared.

Keywords Hairpin vortices, In-line twin synthetic jets, Phase difference, Dye visualization, Particle image velocimetry

1 Introduction

Synthetic jet actuator (SJA), also known as a zero-net-mass-flux actuator, provides a novel means of flow separation control due to its ability to inject non-zero momentum to external flow without net mass flux (Amitay et al 1997; Smith and Glezer 1998; Tang et al 2014; Zhong et al 2007). A typical SJA consists of a cavity with an oscillatory diaphragm on its bottom side and an orifice on the opposite. The diaphragm's periodic downward and upward motion generates a succession of vortex rings that propagates away from the orifice, synthesizing a jet called "synthetic jet" (SJ).

When an SJ is deployed in a crossflow, the streamwise vortices produced through the interaction of the SJ with the crossflow are capable of delaying flow separation by entraining outer high-momentum fluid and enhancing the mixing in the boundary layer (Crook and Wood 2001; Ramasamy et al 2010; Zhong and Zhang 2013). Studies have shown that these vortex structures are complex, varying from hairpin vortices, stretched vortex rings, to tilted vortex rings at different jet-to-crossflow velocity ratio and dimensionless stroke length (Jabbal and Zhong 2008; Zhou and Zhong 2010). It was further found that hairpin vortices and stretched vortex rings are more capable of flow separation control because they are closer to the wall (Jabbal and Zhong 2010; Zhang and Zhong 2010). Besides SJ-induced hairpin vortices, it has also been demonstrated in various experimental and numerical studies that momentum transportation and flow mixing in boundary layers can be enhanced by hairpin vortices either induced by passive control devices (Acarlar and Smith 1987) or auto-generated in turbulent boundary layers (Adrian 2007; Zhou et al 1999).

Hairpin vortices induced by single SJs in laminar boundary layers have been well investigated and fully understood (Jabbal and Zhong 2010; Wen and Tang 2014). Although some studies also revealed that the interaction of multiple SJs leads to more complex vortex structures (Iai et al 2010; Liddel et al 2005; Liddel and Wood 2005), little attention was paid on the interaction of hairpin vortices induced by multiple SJs. To improve the understanding in this aspect, therefore, in the present research we aim to study the interaction of hairpin vortices induced by in-line twin SJs in a laminar boundary layer. More specifically, the effects of operational phase difference between two identical SJAs on the interaction of hairpin vortices are investigated using both stereoscopic dye visualization and particle image velocimetry (PIV) measurements. Rather than focusing on the flow control aspects like what existing investigations typically do, the present study mainly looks at the vortex dynamics of in-line twin SJs in a qualitative sense. Although PIV is a quantitative method, its results are mainly analyzed qualitatively to provide vortex information that is not easy to obtain from the dye visualization.

2 Experimental Approaches

2.1 Test rig

The investigation was conducted in a low-speed water tunnel with a test section of 1 m (L) × 0.45 m (W) × 0.45 m (H). The laminar boundary layer is generated along a long test plate as shown in Fig. 1a, which consists of two smaller flat plates of 10-mm thickness and 430-mm width. The upstream plate is 600-mm long and the downstream plate is 150-mm long. The angle between these two plates was fixed at 180°, such that the total length of the flat plate for the present study is 750 mm. To prevent flow separation at the leading edge, a 1:5 elliptical edge was manufactured on the upstream plate.

Two identical SJAs were designed and installed on the test plate in such a way that their orifices face downward and the resulting SJs appear underneath the plate, as indicated in the side view of Fig. 1a. Each SJA consists of a cylindrical cavity of diameter $D_c = 82$ mm and height $H = 25$ mm, with an orifice plate at one end and a moving diaphragm clamped at the other. The circular orifice has a diameter of $D_o = 5$ mm and a depth of $h = 5$ mm. The diaphragm is made of a thin rubber sheet, whose central portion is sandwiched by two metal plates of diameter $D_d = 45$ mm. The metal plates are attached to a permanent magnetic shaker via a steel rod. By controlling the motion of the shaker, the diaphragm oscillates in a sinusoidal manner at preset amplitudes and frequencies. A 2.5-mm gap between the moving metal plates and their surrounding base plates ensures a piston-like motion of the diaphragm. Two such SJAs are closely located and aligned in line with the crossflow. The distance between the two orifice centers was designed to be adjustable, but in the present study it was kept at a fixed value of $d = 10$ mm or $2D_o$, as depicted in Fig. 1b. These two SJAs are located at 470 mm downstream from the test plate's leading edge, measured at the midpoint of the two orifice centers. This distance allows sufficient development of the laminar boundary layer.

While the operating amplitudes and frequencies of the two SJAs were kept the same in the present study, their phase difference was varied. This was realized by controlling the two individual shakers through Labview. An eddy current displacement sensor was used to read the diaphragm's instantaneous displacement for the purpose of estimating the SJ velocity using Eq. 2 given in Section 2.2.
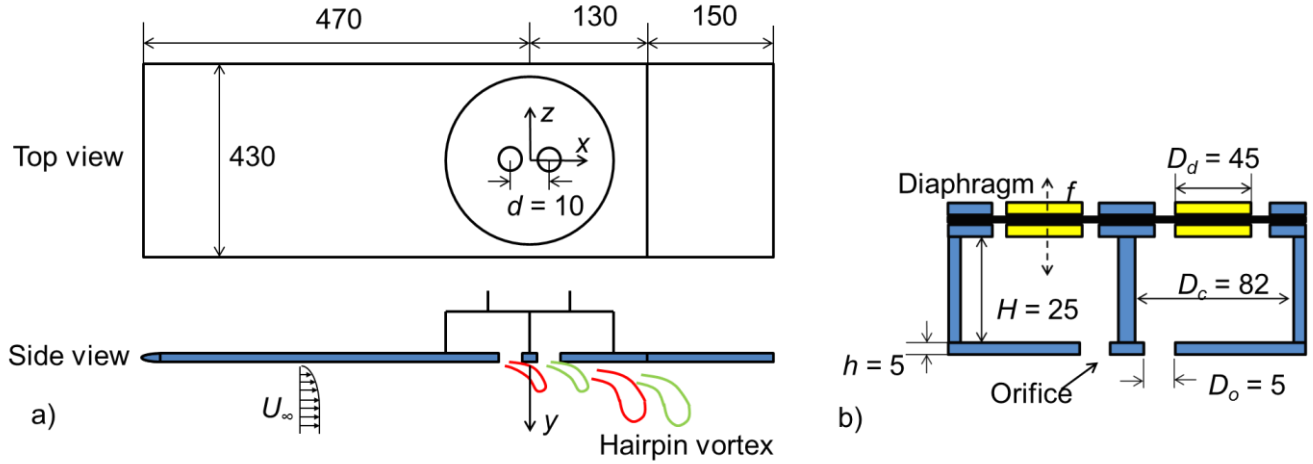

Fig. 1 Schematic of (a) the test plate and (b) the twin SJAs (not to scale; all numbers are in mm)

Both dye visualization and PIV measurements were utilized in the present study. During the tests, the SJA cavities were fully submerged in water. For the dye visualization, before switching on the SJAs the cavities were filled with dyes, which comprise of a mixture of food coloring and methanol. To help differentiate the SJs issued from different SJAs, the upstream cavity was filled with red-color dye and the downstream cavity filled with green-color dye. Two cameras were used to capture the dyed flow structures from two different views, i.e., side view and bottom view, as shown in Fig. 2a. Both cameras operated at the same frame rate of 60 fps, providing stereoscopic dye visualization for the twin SJ interaction.

The PIV measurements were conducted in a spanwise-wall-normal plane at $x = 8D_o$ as shown in Fig. 2b. To facilitate the PIV measurements, the entire water tunnel was seeded with Dantec Dynamics polyamide seeding particles with a mean diameter of 20 μm and a density of 1030 kg/m³. The seeding particles were chosen because their density is similar to water's, so that they are able to accurately follow the flow regardless of their size (Hjelmfelt and Mockkros 1966; Mei 1996). A laser sheet of approximately 1-mm thickness was generated by a 200-mJ double pulsed Nd:YAG laser to illuminate the seeding particles. A FlowSense 2M CDD camera equipped with a Nikon 105mm lens was used to capture a field of view of $y = 0 \sim 4D_o$ and $z = -4D_o \sim 4D_o$ (the coordinate system is shown in Fig. 1a). The velocity vectors were

resolved using a two-frame cross-correlation algorithm, in which a 16×16 pixel interrogation area with an overlap ratio of 50% was chosen, giving a 0.55-mm spatial separation between adjacent vectors. A Labview virtual instrument was used to generate synchronized sinusoidal waveforms for the SJA diaphragms and TTL signals for the PIV timing controller, respectively, so as to start shooting the laser at a selected phase of diaphragm movement, i.e., the maximum blowing of SJA. Phase-averaged results were obtained from 60 instantaneous image pairs, and time-averaged results were obtained by averaging the phase-averaged results of eight equally distributed phases. With the velocity field obtained from the PIV measurements, the streamwise vorticity field can be calculated in the spanwise-wall-normal plane using $\omega_x = \partial u_z/\partial y - \partial u_y/\partial z$ with the central difference scheme, where u_y and u_z are y-component and z-component velocities, respectively. The PIV measurement uncertainties determined from the recursive image interrogation procedure are approximately 2.0% and 5.6% for the velocity and vorticity, respectively, where the uncertainty in vorticity e_ω is evaluated based on the uncertainty in velocity $e_u(= 2.0\%)$, the grid size Δx, and the maximum velocity u_{max} and vorticity ω_{max} in the field, through the formula $e_\omega = (u_{max}\cdot e_u/\Delta x)/\omega_{max}$. In addition, the error associated with the phase-averaging was also estimated through a convergence study. It was found that, compared to using 100 samples for the phase-averaging, using 60 samples only produced an error of less than 1% in the peak velocity in the field.
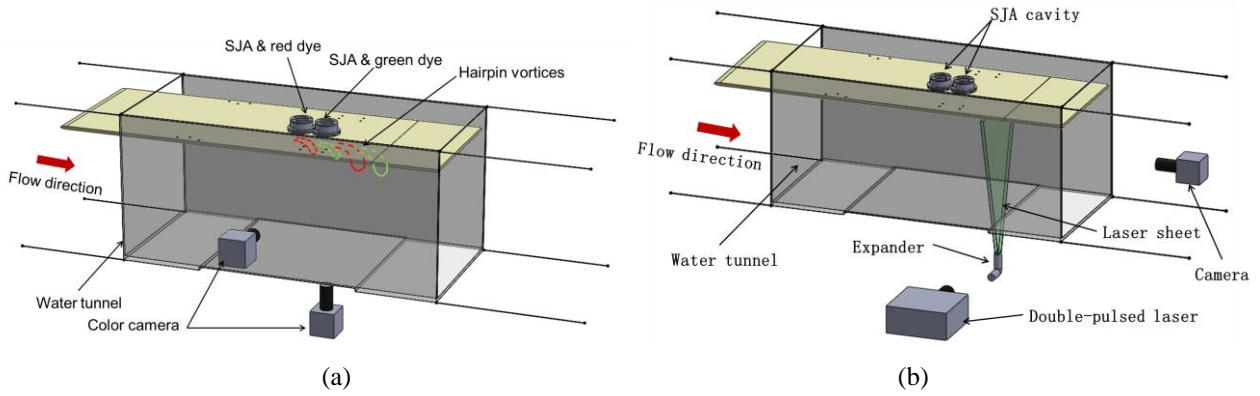

(a)   (b)

Fig. 2 Schematic of the setup for (a) dye visualization and (b) PIV measurement

2.2 Test conditions

In this study, the crossflow velocity was kept at $U_\infty = 0.11$ m/s. A laminar boundary layer is developed along the test plate, and at the SJA orifice exit the boundary layer thickness is 10 mm and the momentum thickness based Reynolds number is $Re_\theta \approx 150$. Although not presented, the measured velocity profile in the boundary layer without the SJs coincides with the Blasius solution, confirming the nature of the present zero-pressure-gradient laminar boundary layer.

According to Jabbal and Zhong (2008), the resulting flow structure of a single SJ issued into a laminar boundary layer is mainly determined by two dimensionless parameters, i.e., the non-dimensional stroke length, L, and jet-to-crossflow velocity ratio, VR. L is defined as

$$L = \frac{L_o}{D_o} = \frac{\bar{U}_o}{fD_o} \tag{1}$$

where L_o is the stroke length representing the length of the fluid column expelled during the SJ blowing stroke, and $\bar{U}_o$ is the time-averaged blowing velocity over an entire actuation cycle. In the present study, the flow is assumed incompressible. Hence $\bar{U}_o$ can be estimated as

$$\bar{U}_o = \Delta f (\frac{D_d}{D_o})^2 \tag{2}$$

where Δ is the diaphragm's peak-to-peak displacement and f the oscillating frequency. The jet-to-crossflow velocity ratio VR is defined as

$$VR = \frac{\bar{U}_o}{U_\infty} \tag{3}$$

which quantifies the relative strength between the jet and crossflow. Similar to the momentum coefficient used in many literature (Milanovic and Zaman 2005), the velocity ratio determines the trajectory of SJs when they penetrate boundary layers (Jabbal and Zhong 2008; Zhong et al 2005): a small VR value indicates a trajectory closer to the wall.

As revealed by Jabbal and Zhong (2008), depending on the *L* and *VR* values, three types of vortex structures can be induced by a single SJ issued into a laminar boundary layer, i.e., hairpin vortices, stretched vortex rings, and tilted vortex rings. It was also found that hairpin vortices are induced at about $1.5 < L < 3.5$ and $0.1 < VR < 0.3$. Therefore, in this research the SJA operating conditions were tuned accordingly: the diaphragm's peak-to-peak displacement was set as $\Delta = 0.105$ mm and the oscillating frequency set as $f = 2$ Hz. From Eqs. 1 to 3, these settings yield $L \approx 1.7$ and $VR \approx 0.16$, at which hairpin vortices are supposed to be produced. Note that since the present study focuses only on vortex dynamics, the velocity ratio of selected twin SJs is quite different from $VR \approx 1$ in many previous research where the focus was on the SJ-based flow separation control (e.g. Vasile and Amitay 2013, Feero et al. 2014, Tang et al. 2014).

3 Results and Discussion

3.1 Single SJs in a laminar boundary layer

Before the interaction of the in-line twin SJs is investigated, the flow pattern of single SJs in the laminar boundary layer is discussed as a baseline case. As expected, hairpin vortices are generated under the present test conditions, with a clear hairpin head followed by a pair of hairpin legs as showed in the two views of Fig. 3a. The formation of these hairpin vortices is a direct result of the interaction between the SJ and the boundary layer. In quiescent conditions, vortex rings will be produced from the SJA orifice. As explained by Zhong et al. (2005), when a crossflow is introduced, the upstream branch of the vortex ring is weakened by the opposite-signed resident vorticity in the boundary layer. Due to the Magnus effect, the vortex ring gradually tilts towards downstream, with its upstream branch becoming closer to the wall than its downstream branch. As the flow structure develops further, the upstream branch vanishes and the downstream branch starts getting stretched under the shear stress in the boundary layer. As such, a hairpin vortex forms. Although this formation process is not presented in the figure, the well-defined vortex tubes that form the hairpin vortex are captured in the side view of the dye visualization, indicating the laminar nature of the flow structures. The hairpin head penetrates the boundary layer within two SJ actuation cycles, after which the hairpin head becomes upright due to much less shear stress out there, as demonstrated by the downstream hairpin vortex in Fig. 3a.

The time sequence of PIV measurements in the $x = 8D_o$ plane also captures the passage of the hairpin vortex. By arranging snapshots of vorticity contours in that plane at eight equally distributed phases along a time axis, the hairpin vortex can be re-constructed as demonstrated in Fig. 3b. With this method, the hairpin leg is well captured, which is defined by contours of large positive (in red) or negative (in blue) streamwise vorticity values. As shown by the double dashed lines, the shape of the "captured" hairpin vortex generally looks similar to that shown in the dye visualization. Additional vortex structures that are not captured in the dye visualization are also captured in the present PIV results. As shown in Fig. 3b, a pair of secondary vortices underneath the hairpin legs is captured, which carries vorticity opposite in sign to the hairpin legs. As explained by Wen and Tang (2014), these secondary vortices are partially induced by the hairpin legs and partially induced by the SJA ingestion stroke.
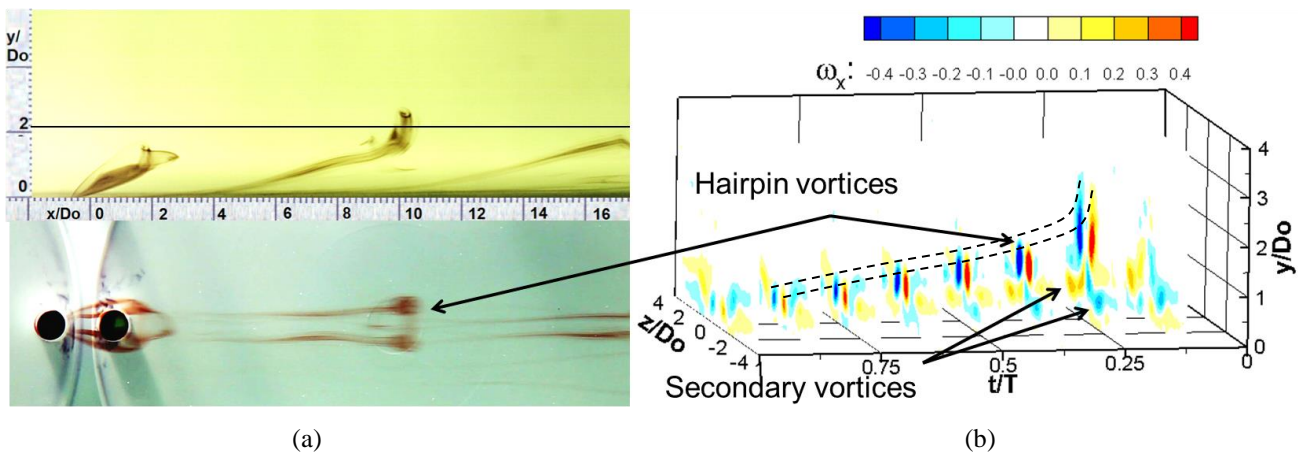

Fig. 3 (a) Stereoscopic dye images of a single SJ in a laminar boundary layer. The horizontal line in the side view indicates the edge of the boundary layer. (b) Snapshots of streamwise vorticity contour in the plane $x = 8D_o$ during an actuation cycle.

4

3.2 Interaction of in-line twin SJs at various phase differences

The interaction of the two SJ-induced hairpin vortices in the laminar boundary layer were investigated by varying the phase difference between the two SJAs. Here the phase difference is defined as $\Delta\phi = \phi_u - \phi_d$, where ϕ_u and ϕ_d are the operational phases of the upstream and downstream SJAs, respectively. Four different phase differences, i.e., $\Delta\phi = 0°$, 90°, 180° and 270°(or –90°), were studied. Fig. 4 shows the dye visualization results. The vortex structures in red are generated from the upstream SJA and those in green are generated from the downstream SJA. Three different types of vortex structures were observed, i.e., *one combined vortex* at $\Delta\phi = 90°$, *two completely separated hairpin vortices* at $\Delta\phi = 270°$, and *partially interacting vortex structures* at $\Delta\phi = 0°$ and 180°.

At $\Delta\phi = 90°$, the downstream-SJA produced vortex emerges when its upstream-SJA produced counterpart just passes by, forming the leftmost vortex structure in Fig. 4b. These two vortices perfectly merge together and form a new vortex structure. Instead of being a hairpin vortex, this new vortex structure seems more like a tilted vortex ring that penetrates the boundary layer much faster than the single-SJ produced hairpin vortex (Fig. 3a). The increased size and concentration of swirling lines inside the new vortex head also indicate the increase of the vortex strength. Hence at this phase difference, the two hairpin vortices interact in a constructive manner in terms of the vortex size, strength, and celerity.

At $\Delta\phi = 270°$, the downstream-SJA produced hairpin vortex appears when its upstream-SJA produced counterpart has passed the downstream SJA for about half an actuation cycle, i.e., $T/2$. Hence the newly produced hairpin vortex is not affected too much and looks very similar to the single-SJ produced hairpin vortex. As demonstrated in Fig. 4d, the resulting flow structures are then a train of hairpin vortices with the same color appearing in an alternate way, like doubling the frequency of the single-SJ produced hairpin vortex. It is interesting to see that the hairpin legs in the present case are much closer to the wall, leaving a significant portion of dye in the near-wall region. Furthermore, the tip of each hairpin leg is lifted up and entrained by its following hairpin vortex, forming a wake-like flow pattern in the near-wall region.
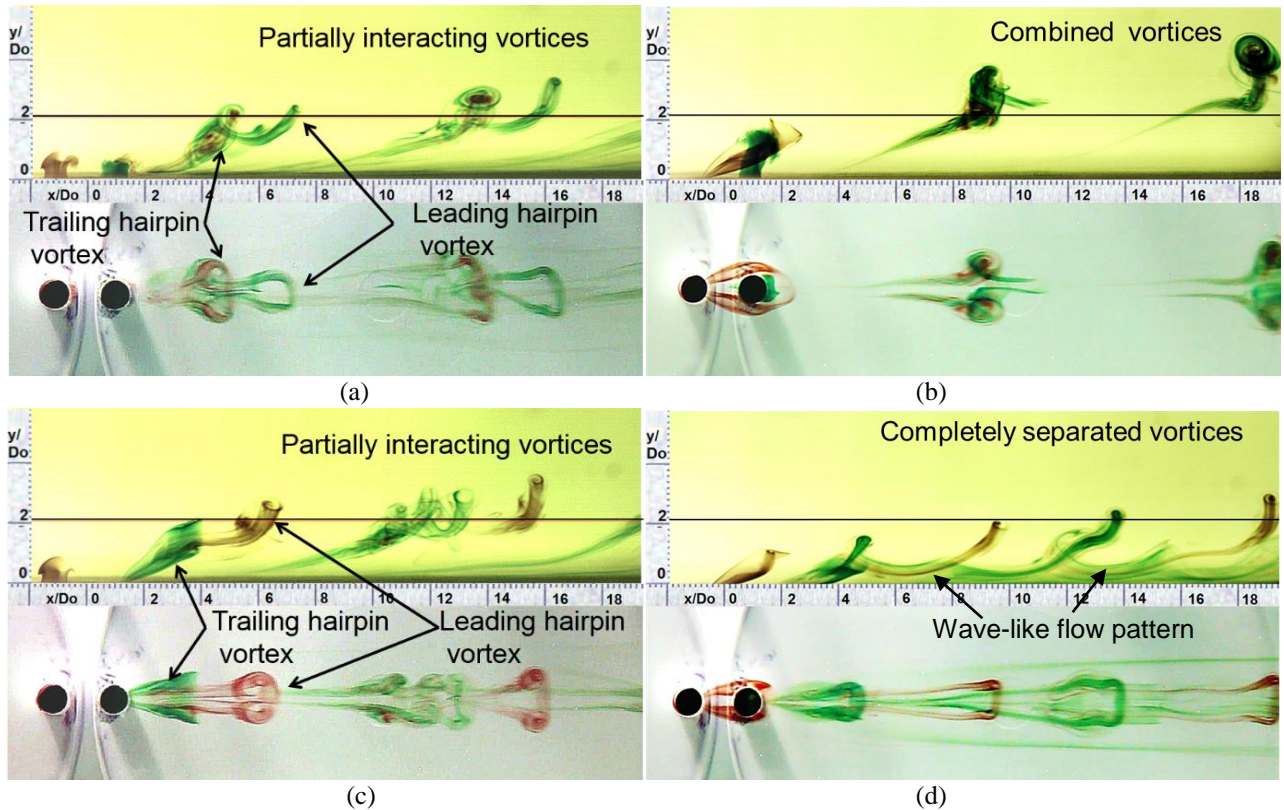

Fig. 4 Stereoscopic dye images of the in-line twin SJs at $\Delta\phi =$ (a) 0°, (b) 90°, (c) 180° and (d) 270°

At the other two phase differences, i.e., $\Delta\phi = 0°$ and 180°, the two hairpin vortices are not merged but close enough, with the head of one hairpin vortex coupled with the leg of the other, forming complex vortex structures as shown in Fig. 4a and 4c. The time difference between these two hairpin vortices is about a quarter of an actuation cycle, i.e., $T/4$. As shown in Fig. 4a, at $\Delta\phi = 0°$ the upwash flow induced between the two legs of the trailing hairpin vortex (in red) lifts up the mid

portion of the leading hairpin legs (in green). A part of the lifted-up legs is even entrained into the head of the trailing hairpin vortex, making the latter continue growing in size. Things are a little different at $\Delta\phi = 180°$. The trailing hairpin head (in green) is significantly disturbed by the leading hairpin legs (in red) and has no time to develop its own coherence. Hence it is broken up into multiple small vortex heads as shown in Fig. 4c. And because of the disturbance, the flow pattern of the trailing hairpin vortex is not perfectly laminar but a little bit turbulent. In contrary, at $\Delta\phi = 0°$ the trailing hairpin head issued from the upstream SJA (in red) seems not affected too much and is able to maintain its coherence. As for the leading hairpin vortex, the one issued from the upstream SJA at $\Delta\phi = 180°$ (Fig. 4c, in red) is more sustained than the one issued from the downstream SJA at $\Delta\phi = 0°$ (Fig. 4a, in green). The comparison indicates that, regardless the phase difference, the hairpin vortices issued from the upstream SJA are able to maintain their coherence more easily than their counterparts issued from the downstream SJA.

The PIV measurements are not only able to capture the aforementioned three types of vortex structures, but also able to capture secondary vortices underneath the hairpin legs, which however did not appear in the dye visualization. It is believed that the secondary vortices together with the hairpin legs are able to bring outer high-momentum fluid into the near-wall region, and hence delay flow separation. Therefore, the present PIV analysis will be focused on the similarity and difference of the primary vortices as well as the secondary vortices at the four phase differences, as shown in Fig. 5. Note in each sub-figure, $t/T = 0$ was chosen in such a way that the integrity of flow structures produced in one actuation cycle is kept.
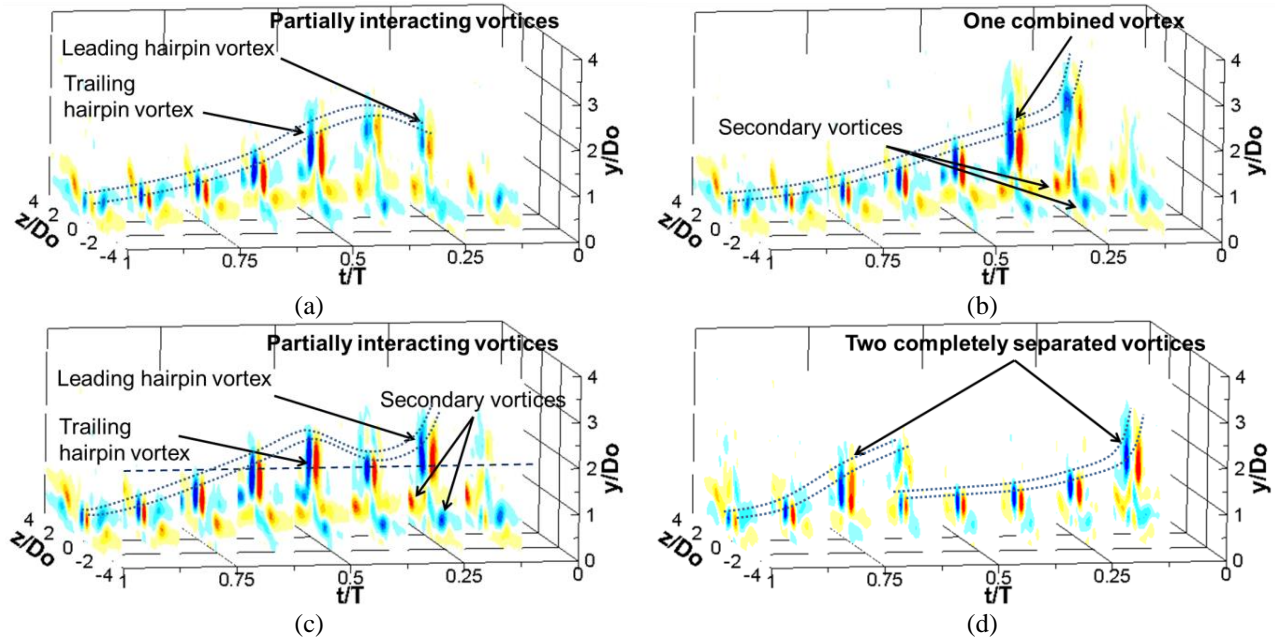

Fig. 5 Contour of streamwise vorticity in the $x = 8D_o$ plane in one actuation cycle at $\Delta\phi = $ (a) $0°$, (b) $90°$, (c) $180°$ and (d) $270°$. Refer to Fig. 3 for the color map

In Fig. 5b at $\Delta\phi = 90°$, a single, large vortex is captured, which stays highest among all of the four cases. At $\Delta\phi = 270°$ as shown in Fig. 5d, the actuation cycle includes two smaller duplicated cycles, indicating the occurrence of two completely separated hairpin vortices. At $\Delta\phi = 0°$ as shown in Fig. 5a, the partially interacting vortex structures are not so obvious, in which the trailing hairpin vortex is dominant whereas the leading hairpin vortex shown in the $t/T = 0.25$ plane is weak. On the contrary, at $\Delta\phi = 180°$ as shown in Fig. 5c, the shape of partially interacting vortex structures is very clear, with the leading hairpin vortex well captured at $t/T = 0.25$ and 0.375 and the trailing hairpin vortex well captured at $t/T \geq 0.5$. The significant difference in the strength of the leading hairpin vortex at $\Delta\phi = 0°$ and $180°$ stems from the formation phase of the twin hairpin vortices. At $\Delta\phi = 0°$, the trailing hairpin vortex from the upstream SJA shields its counterpart from the boundary layer flow all the way. As the resident vorticity in the boundary layer can strengthen the hairpin vortex (Jabbal and Zhong 2008), this shielding effect suppresses the growth of the leading hairpin vortex from the downstream SJA. At $\Delta\phi = 180°$, on the contrary, during its formation the leading hairpin vortex produced by the upstream SJA does not experience the shielding effect, and hence is able to sustain its coherence in the following interactions (Honami and Motosuke 2012). This observation is consistent with what has been observed in the dye visualization, in which the leading hairpin vortex at

6

$\Delta\phi = 0°$ (in green shown in Fig. 4a) seems much weaker than that at $\Delta\phi = 180°$ (in red shown in Fig. 4c) if observed from the top view.

In Fig. 5, a pair of smaller regions of vorticity concentration in the near-wall region, with vorticity opposite in sign to the hairpin legs, defines the secondary vortices. Located underneath and outboard of the hairpin legs, they are induced by the hairpin legs. It is seen that one combined vortex induces obviously stronger secondary vortices at $\Delta\phi = 90°$ than that induced by two completely separated hairpin vortices at $\Delta\phi = 270°$.

Time-averaged streamwise vorticity in the $x = 8D_o$ plane was also obtained by averaging velocity fields of the eight phases in one actuation cycle. Fig. 6 shows its contour superimposed by velocity vectors for the twin SJ cases of four phase differences and for the single SJ case. Compared to the single SJ, the twin SJs regardless of the phase difference are able to produce stronger or larger primary and secondary vortices. Among the four twin SJ cases, the case at $\Delta\phi = 90°$ shows the highest primary vortices as a result of formation of the combined vortex structures. However, because of their low occurrence rate and inclined vortex legs these primary vortices are relatively weaker in terms of vorticity strength. At $\Delta\phi = 270°$, the primary vortices stay lowest, even lower than the single hairpin vortex. But they are much stronger in the time-average sense, mainly because of their doubled occurrence rate. As for the two cases showing time-averaged partially interacting vortex structures, the structures are very strong at $\Delta\phi = 180°$ but weak at $\Delta\phi = 0°$. The clear core of the primary vortex in the $\Delta\phi = 180°$ case is located around $y = 1.5D_o$, as shown in Fig. 6c. At this height it can be seen from Figs. 4c and 5c that the major portion of the partially interacting vortex structure passes through the $x = 8D_o$ plane almost parallel to the wall (as indicated by the horizontal dashed line in Fig. 5c), hence resulting in a strong time-averaged vorticity. As for the time-averaged secondary vortices, strong vorticity values appear at $\Delta\phi = 0°$, $90°$ and $180°$. The velocity vectors confirm that, in the time-averaged sense, SJs introduce an upwash flow between the two counter-rotating hairpin legs, and downwash flows outboard and underneath the legs.
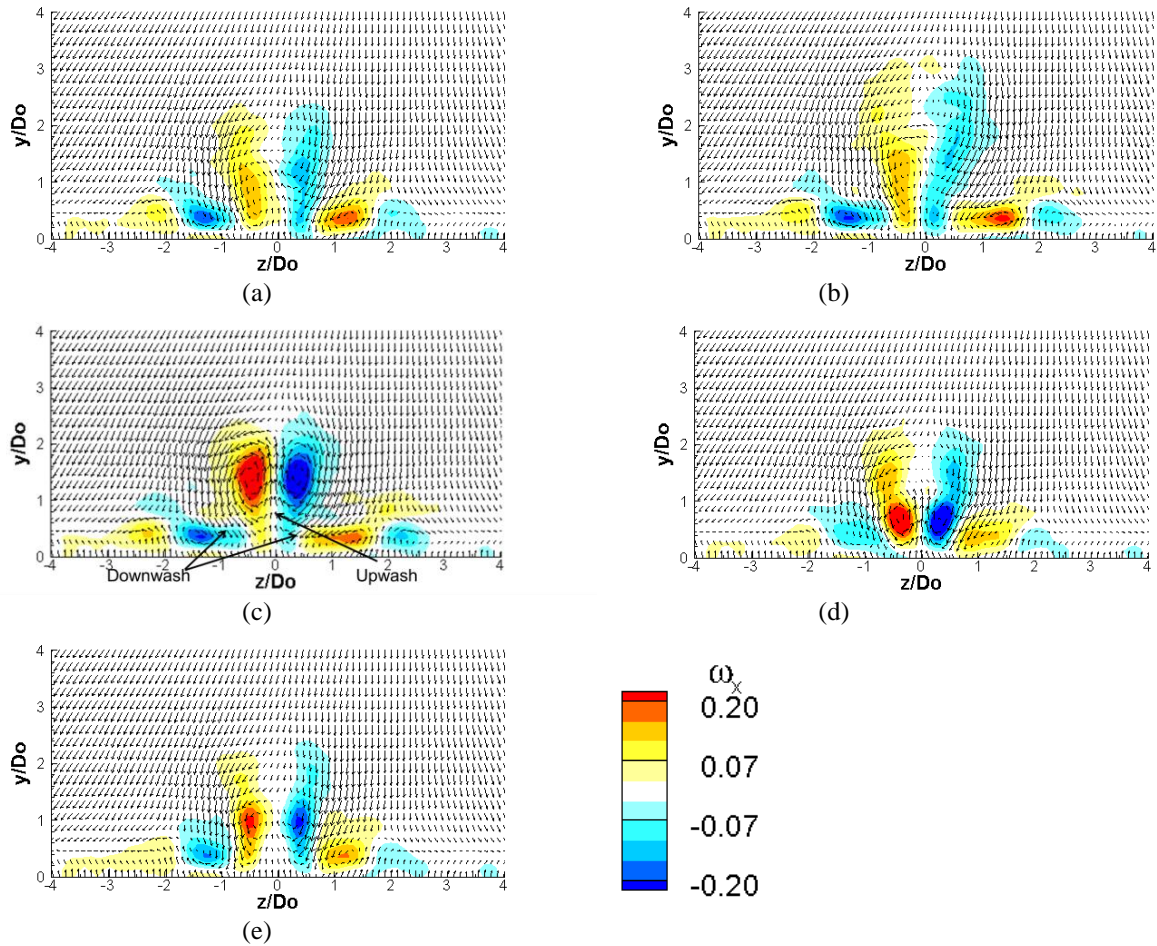

Fig. 6 Contour of time-averaged streamwise vorticity in the $x = 8D_o$ plane at $\Delta\phi =$ (a) 0°, (b) 90°, (c) 180°, (d) 270°, and for (e) single SJ

4 Conclusions

This experimental study investigated the effect of operational phase difference of in-line twin SJAs on the interaction of SJ-induced hairpin vortices in a laminar boundary layer along a flat plate. Both stereo dye visualization and PIV techniques were utilized. The resulting vortex structures at four phase differences, i.e., $\Delta\phi = 0°$, $90°$, $180°$, and $270°$, were presented and compared. Three types of vortex structures were observed: *one combined vortex* at $\Delta\phi = 90°$, *two completely separated hairpin vortices* at $\Delta\phi = 270°$, and *partially interacting vortex structures* at $\Delta\phi = 0°$ and $180°$. The combined vortex is the strongest and most penetrates into the boundary layer. Although each individual hairpin vortex is weak, the completely separated hairpin vortices are the closest to the wall and hence are able to exert the most influence in the near-wall region in the time-average sense. As for the partially interacting vortex structures, the head of one hairpin vortex interacts with the leg of the other, producing complex flow structures. However, the flow structures at $\Delta\phi = 0°$ is somewhat different from those at $\Delta\phi = 180°$. Through this investigation it was also found that the hairpin vortices issued from the upstream SJA are able to maintain their coherence more easily than their counterparts issued from the downstream SJA, regardless the phase difference. The secondary vortices captured by the PIV measurements were also showed and compared. These secondary vortices are located underneath and outboard of the primary hairpin legs, and show strong vorticity values at $\Delta\phi = 0°$, $90°$ and $180°$.

References

1. Acarlar MS, Smith CR (1987) A study of hairpin vortices in a laminar boundary layer. Part 1. Hairpin vortices generated by a hemisphere protuberance. J. Fluid Mech. 175:1-41
2. Adrian RJ (2007) Hairpin vortex organization in wall turbulence. Phys. Fluids 19:041301
3. Amitay M, Honohan A, Trautman M, Glezer A (1997) Modification of the aerodynamic characteristics of bluff bodies using fluidic actuators. AIAA Paper 97-2004
4. Crook A, Wood NJ (2001) Measurements and visualisations of synthetic jets. AIAA Paper 2001-0145
5. Feero MA, Goodfellow S.D, Lavoie P, Sullivan PE (2014) Flow reattachment using synthetic jet actuation on a low-Reynolds-number airfoil. AIAA J., articles in advance, pp. 1-10, Dec. 2014
6. Hjelmfelt AT Jr, Mockros LF (1966) Motion of discrete particles in a turbulent fluid. Appl. Sci. Res. 16:149-161.
7. Honami S, Motosuke M (2012) Vortex interaction of in-lined synthetic jets injected at different phase in low Reynolds number cross flow. AIAA Paper 2012-3243
8. Iai T, Iwabuchi K, Motosuke M, Honami S (2010) Vortex behavior of in-line synthetic jets in cross flow. AIAA Paper 2010-4412
9. Jabbal M, Zhong S (2008) The near wall effect of synthetic jets in a boundary layer. Int. J. Heat Fluid Flow 29:119-130
10. Jabbal M, Zhong S (2010) Particle image velocimetry measurements of the interaction of synthetic jets with a zero-pressure gradient laminar boundary layer. Phys. Fluids 22:063603
11. Mei R (1996) Velocity fidelity of flow tracer particles. Exp. Fluids 22:1-13
12. Milanovic IM, Zaman KBMQ (2005) Synthetic jets in crossflow. AIAA J. 43(5):929-940
13. Milanovic IM, Zaman KBMQ, Rumsey CL (2005) An isolated circular synthetic jet in cross-flow at low momentum-flux ratio. AIAA Paper 2005-1110
14. Ramasamy M, Wilson JS, Martin PB (2010) Interaction of synthetic jet with boundary layer using microscopic particle image velocimetry. J. Aircraft 47(2):404-422
15. Smith BL, Glezer A (1998) The formation and evolution of synthetic jets. Phys. Fluids 10(9):2281-2297
16. Tang H, Salunkhe P, Zheng Y, Du J, Wu, Y (2014) On the use of synthetic jet actuator arrays for active flow separation control. Exp. Therm. Fluid Sci. 57:1-10
17. Vasile JD, Amitay M (2013) Interactions of an array of finite span synthetic jets and a crossflow. AIAA J. 51:2503-2512
18. Wen X, Tang H (2014) On hairpin vortices induced by circular synthetic jets in laminar and turbulent boundary layers. Comput. Fluids 95:1-18
19. Zhang S, Zhong S (2010) Experimental investigation of flow separation control using an array of synthetic jets. AIAA J. 48(3):611-623
20. Zhong S, Jabbal M, Tang H, Garcillan L, Guo F, Wood N, Warsop C (2007) Towards the design of synthetic-jet actuators for full-scale flight conditions. Flow Turbul. Combust. 78:283-307
21. Zhong S, Millet F, Wood NJ (2005) The behaviour of circular synthetic jets in a laminar boundary layer. Aeronaut. J 109:461-470
22. Zhong S, Zhang S (2013) Further examination of the mechanism of round synthetic jets in delaying turbulent flow separation. Flow Turbul. Combust. 91:177-208

23. Zhou J, Adrian RJ, Balachandar S, Kendall TM (1999) Mechanisms for generating coherent packets of hairpin vortices in channel flow. J. Fluids Mech. 387:353-396
24. Zhou J, Zhong S (2010) Coherent structures produced by the interaction between synthetic jets and a laminar boundary layer and their surface shear stress patterns. Comput. Fluids 39:1296-1313